Large-scale neuroimaging and genetic study reveals genetic architecture of brain white matter microstructure

Bingxin Zhao, M.S.[1], Jingwen Zhang, B.S.[1], Joseph G. Ibrahim, Ph.D.[1], Rebecca C. Santelli, Ph.D.[2], Yun Li, Ph.D.[1,3,4], Tengfei Li, Ph.D.[5], Yue Shan, B.S.[1], Ziliang Zhu, B.S.[1], Fan Zhou, M.S.[1], Huiling Liao. B.S.[6], Thomas E. Nichols, Ph.D.[7,8], Paul M. Thompson, Ph.D.[9], and Hongtu Zhu, Ph.D.*[1,5]

[1]Departments of Biostatistics, [2] Psychiatry, [3] Genetics, and [4]Computer Science, University of North Carolina at Chapel Hill, Chapel Hill, NC, USA, 27599

[5] Department of Biostatistics, The University of Texas MD Anderson Cancer Center, Houston, TX, USA, 77230

[6] Department of Statistics, Texas A&M University, College Station, TX, USA, 77843

[7] Wellcome Trust Centre for Integrative Neuroimaging, Big Data Institute, University of Oxford, Oxford, UK, OX1 2JD

[8] Department of Statistics, University of Warwick, Coventry, UK, CV4 7AL

[9] Imaging Genetics Center, Mark and Mary Stevens Institute for Neuroimaging & Informatics, University of Southern California, Los Angeles, CA, USA, 90033

Corresponding author:

Hongtu Zhu

Full postal address: Department of Biostatistics, The University of Texas MD Anderson Cancer Center, 1515 Holcombe Blvd, Unit 1411, Houston, TX 77030, Telephone number: 832-750-4931, Fax number: 832-750-4931, Email address: hzhu5@mdanderson.org

List of Pediatric Imaging, Neurocognition and Genetics (PING) authors provided in the supplemental materials.

Version: March 24, 2018

Abstract

Microstructural changes of white matter (WM) tracts are known to be associated with various neuropsychiatric disorders/diseases. Heritability of structural changes of WM tracts has been examined using diffusion tensor imaging (DTI) in family-based studies for different age groups. The availability of genetic and DTI data from recent large population-based studies offers opportunity to further improve our understanding of genetic contributions. Here, we analyzed the genetic architecture of WM tracts using DTI and single-nucleotide polymorphism (SNP) data of unrelated individuals in the UK Biobank (n ~ 8000). The DTI parameters were generated using the ENIGMA-DTI pipeline. We found that DTI parameters are substantially heritable on most WM tracts. We observed a highly polygenic or omnigenic architecture of genetic influence across the genome as well as the enrichment of SNPs in active chromatin regions. Our bivariate analyses showed strong genetic correlations for several pairs of WM tracts as well as pairs of DTI parameters. We performed voxel-based analysis to illustrate the pattern of genetic effects on selected parts of the tract-based spatial statistics skeleton. Comparing the estimates from the UK Biobank to those from small population-based studies, we illustrated that sufficiently large sample size is essential for genetic architecture discovery in imaging genetics. We confirmed this finding with a simulation study.

Keywords: SNP heritability; White matter tract; Tract-based spatial statistics skeleton; UK Biobank; Genetic architecture

Complex brain functions rely on dynamic interactions between distributed brain areas operating in large-scale networks. Consequently, the integrity of white matter connections between brain areas is critical to proper function. Microstructural differences in white matter (WM) tracts are associated with information processing speed and intelligence (1-5) as well as neuropsychiatric diseases and disorders, such as Alzheimer's disease (6), schizophrenia (7), attention-deficit/hyperactivity disorder (8) and anorexia nervosa (9). A better understanding of factors influencing integrity of WM tracts could have important implication for understanding the etiology of these diseases as well as

individual variation in intelligence. To reveal the underlying genetic contributions to human brain structure/function development and disease/disorder processes, the study of imaging genetics on WM microstructure has been an active area of research over the past fifteen years. The structural changes of WM tracts are usually measured and quantified in diffusion tensor imaging (DTI; (10)). Brain diffusivity can be influenced by many aspects of its micro- or macro-structures (11). To reconstruct the WM pathways and tissue microstructure, DTI models the diffusion properties of WM using the random movement of water. Specifically, DTI quantifies diffusion magnetic resonance imaging (dMRI) in a tensor model, which allows us to calculate diffusions in all directions. A typical DTI diagonalizes the tensor and calculates three pairs of eigenvalues/eigenvectors that respectively represent one primary and two secondary diffusion directions. Within each voxel, several DTI parameters can be derived from these eigenvalues: fractional anisotropy (FA) and the mean (MD), axial (AD), and radial (RD) diffusivities. FA is the normalized variance of these three eigenvalues that represents the directional diffusion. As a summary measure of WM integrity (12, 13), higher FA means stronger directionality in this voxel. MD is the mean of the three eigenvalues, which quantifies the magnitude of absolute directionality. AD is essentially the eigenvalue of the principal direction, and RD is the average of the eigenvalues of the two secondary directions. The mode of anisotropy (MO), which is the third moment of the tensor, is also an interesting parameter. A positive MO value reflects narrow tubular water diffusion, whereas a negative value denotes planar water diffusion (14). There are several available approaches for analyzing DTI data across the whole brain, including manual region-of-interest (ROI) analysis, automated ROI analysis, voxel-based analysis, such as tract-based spatial statistics (TBSS; (15)), as well as tractography and graph theory analysis; see Tamnes, et al. (16) for a survey.

As an initial step, the magnitude of genetic influences (i.e., heritability) in various DTI parameters of WM tracts, including FA, MD, AD, and RD, has been examined in family-based studies across a wide age range, from neonates (17, 18), young children (19), older children (20, 21), adolescents (22), and young adults (23) to middle aged (24) and older adults (25). The participants in these studies are typically monozygotic and dizygotic twins or family members. Table 1 of Vuoksimaa, et al. (24) lists 14 studies that

illustrated that a substantial proportion of variance in DTI parameters (FA, MD, AD, and RD) was explained by additive genetic effects. However, the genetic architecture of DTI parameters remains largely unknown due to the limitation of family-based studies, for which the heritability estimation has relied on contrasting the phenotypic similarity between monozygotic and dizygotic twins. Genetic architecture denotes the characteristics of genetic variations that contribute to the broad-sense heritability of a phenotype (26). Different heritable human traits may have very different genetic architecture. Based on the number of genetic variants contributing to phenotypic variance, genetic architecture for a specific phenotype can be described as monogenic (one variant), oligogenic (few variants), polygenic (many variants), or onmigenic, which hypothesizes that almost all genetic variants have small but non-zero genetic contributions (27, 28).

The availability of genomic and polygenic data from recent large population-based studies, such as the United Kingdom (UK) Biobank resource (29), offers the opportunity to improve our understanding of genetic architecture. With data from genome-wide association studies on population-based unrelated individuals, recent developments have provided an alternative estimator of heritability by estimating the additive contribution of all common single-nucleotide polymorphisms (SNPs) on phenotypic variance (30-32), which is often termed SNP heritability. Instead of using the expected genetic correlation based on pedigree information, SNP heritability is directly estimated from linear mixed-effect models (LMMs) averaging across all (or a set of) common SNPs (minor allele frequency [MAF] > 0.05 or 0.01). Since SNP heritability captures neither non-additive genetic variation nor genetic variation that is not measured by the selected genotyping microarray, it is usually viewed as a lower bound estimate for narrow-sense heritability (33). Though some concerns remain, SNP heritability has been successfully applied on various human traits, providing us with deeper insights into the genetic basis of these phenotypes; see Yang, et al. (34) for an overview. Heritability is not a fixed property of a phenotype, and its estimation may depend on non-genetic/environmental factors. In addition, as illustrated in our simulation, the variance-component analysis used in SNP heritability estimation usually requires a large sample size. For these reasons, the UK Biobank resource provides a unique opportunity to conduct SNP heritability analysis of brain WM tracts in one large-scale, relatively homogeneous population. The UK

Biobank has captured data from over 500,000 original participants of middle or elderly ages, and is currently in the process of following up with 100,000 of these participants to perform brain MRI screening. Imaging data of the first 10,000 subjects have recently been released for public research access (35).

Here, we used all common (MAF > 0.01) autosomal SNPs to estimate heritability of DTI parameters in 21 main WM tracts, as well as in 42 WM sub-tracts. In addition to FA, AD, RD, MD and MO, we examined the heritability of the two secondary diffusion direction eigenvalues, respectively denoted as L2 and L3. All of these DTI parameters were generated using the ENIGMA-DTI pipeline (36). We also refer to AD as L1, since AD is essentially the eigenvalue of the primary diffusion direction. We partitioned genetic variation into individual chromosomes to examine the distribution of genetic effects across the genome. To assess the enrichment of SNPs in active chromatin regions, we partitioned genetic variation according to cell-type-specific functional annotations (37). We further examined the genetic correlation for several pairs of DTI parameters and their relationship with the corresponding phenotypic correlation across WM tracts. We estimated gender-specific heritability for each DTI parameter in the main WM tracts and mapped the symmetric pattern of heritability in WM sub-tracts in the left and right hemispheres. We also performed voxel-based analysis to illustrate the pattern of genetic effects on selected parts of the TBSS skeleton. Finally, we performed simulations to study the role of sample size in SNP heritability estimation and compared the results obtained from the UK Biobank with those obtained from the Philadelphia Neurodevelopmental Cohort (PNC, n ~ 600; (38)), and Pediatric Imaging, Neurocognition, and Genetics (PING, n ~500; (39)) datasets. The results suggest that a sufficiently large sample size is essential for genetic architecture discovery in future studies.

RESULTS

SNP heritability by all common autosomal SNPs

We first estimated the proportion of individual variability in DTI parameters of WM tracts that can be explained by the additive effects of all common autosomal SNPs. We used the GCTA tool set (30) to estimate the genetic relationship matrix (GRM) for SNP heritability estimation, adjusting for fixed effects of baseline age, sex, and the top 10 genetic principal components.

Figs. 1-2 and Supplementary Figs. 1-8 display the SNP heritability estimates on the 21 main WM tracts. The associated standard errors and p-values from the one-sided likelihood ratio tests are given in **Supplementary Table 1**. We adjusted for multiple testing by using the Benjamini and Hochberg (40) procedure. Genetic factors account for a moderate or large portion of the variance of DTI parameters in almost all WM tracts. For example, genetic effects explained more than 60% of the total variance of FA in the posterior limb of the internal capsule (PLIC), anterior corona radiata (ACR), superior longitudinal fasciculus (SLF), cingulum cingulate gyrus, anterior limb of the internal capsule, and genu of the corpus callosum (GCC); and explained between 60% and 50% of the FA variance in the superior fronto-occipital fasciculus, retrolenticular part of the internal capsule, external capsule, superior corona radiata (SCR), posterior corona radiata, splenium of the corpus callosum (SCC), fornix/stria terminalis, sagittal stratum, inferior fronto-occipital fasciculus, and posterior thalamic radiation. SNP heritability of FA decreased to 28% and 22%, respectively, in the corticospinal tract (CST) and fornix (FX). The heritability in the last two tracts was consistently reported to be low across previous studies (23). The 42 WM sub-tracts, most of which are left/right pairs, also show SNP heritability (**Supplementary Table 1**). Noticeable evidence of symmetry in SNP heritability was observed on the WM sub-tracts (**Supplementary Figs. 9-15**).

The SNP heritability of FA, AD (L1), RD, MD, MO, L2 and L3 is similar to each other on almost all WM tracts. We also estimated sex-specific heritability of each DTI parameter on the 21 main WM tracts (**Supplementary Figs. 16-22**), and found sex-specific modifications on SNP heritability on several WM tracts, but detected no systematic pattern. And the distribution of SNP heritability was largely consistent across all, female, and male individuals. According to the functions of the main WM tracts (Connectopedia Knowledge Database, http://www.fmritools.com/kdb/white-matter/), we

clustered them into four communities: complex fibers (C1), associative fibers (C2), commissural fibers (C3) and projection fibers (C4). We found that the set of WM tracts in C1 and C3 tended to have higher SNP heritability than those in C2 and C4.

Partitioning genetic variation by chromosome

We partitioned the SNP data into individual chromosomes to examine the distribution of SNP heritability across the genome. Specifically, we estimated the GRM using SNPs from each chromosome (22 GRMs in total) and used each of these GRMs separately to estimate the SNP heritability of DTI parameters. We found that the aggregated heritability across all of the 21 main WM tracts explained by each chromosome was linearly associated with the length of the chromosome (**Fig. 3(a)**, R^2= 61.3%, p-value=$1.63*10^{-05}$). These findings reveal a highly polygenic, or omnigenic genetic architecture (28) of WM tracts and that SNPs that contribute to the variation in DTI parameters are widely spread across the whole genome.

To further illustrate this architecture, we ordered and clustered the 22 chromosomes into three groups by their lengths: long, medium, and short. The long group had 4 chromosomes, which together accounted for 33% of the length of the whole genome; the medium group had 6 chromosomes, which accounted for another 33% of the length of the whole genome; and the short group consisted of the remaining 12 chromosomes. **Fig. 3(b)** shows the SNP heritability grouped by chromosomal length for each of the seven DTI parameters. It is clear that longer chromosomes tended to have higher SNP heritability than shorter ones for all DTI parameters.

Partitioning genetic variation by functional annotation

To assess the enrichment of SNPs in active chromatin regions, we partitioned the genetic variation according to cell-type-specific annotations (37, 41). SNPs can be grouped according to their general activeness in various cell groups. In our DTI analysis, we particularly focused on the activeness in the central nervous system (CNS) cell group, and thus clustered all SNPs into three groups: CNS_active, CNS_inactive, and

always_inactive (see Online Methods for detailed definitions). We randomly selected the same number of SNPs from each cell group and computed the heritability for each group in each tract. We found strong evidence that on average SNPs residing in CNS-cell-active chromatin regions (CNS_active) contributed much more to DTI heritability than other SNPs. Moreover, SNPs in chromatin regions that remained inactive across all cell groups (always_inactive) contributed much less to DTI heritability than SNPs residing in chromatin regions that were active in at least one cell group, but not the CNS cell group (CNS_inactive) (**Fig. 4**). This pattern remained consistent across all of the seven DTI parameters, though larger variance was observed for the MO parameter.

Genetic correlation across DTI parameters and WM tracts

In bivariate analyses, we applied the BOLT-REML tool set (31) to estimate the genetic correlation for several pairs of DTI parameters on each of the main WM tracts, adjusting for the same set of covariates as in the univariate analysis. We verified that both FA and RD had positive genetic correlation with AD (L1) on most of the WM tracts, while FA and RD had strong negative correlation on all of the main WM tracts (**Supplementary Fig. 23**). Similarly, L1 had positive genetic correlation with L2 and L3 on many of the main WM tracts, and L2 and L3 had strong positive correlation on all of the main WM tracts (**Supplementary Fig. 24**). We further examined the relationship between these genetic correlations and the corresponding phenotypic correlations across WM tracts. Interestingly, a significant linear association with a slope close to one was found for each of these pairs, which indicates that the estimated genetic correlations are robustly proportional to the phenotypic correlations across WM tracts.

We also estimated the genetic correlation on pairs of the main WM tracts for each DTI parameter (**Fig. 5 and Supplementary Fig. 25**). For MD and RD, substantive genetic correlation was detected on many pairs of WM tracts; for AD (L1) and FA, the genetic correlations were generally smaller compared to those of MD or AD and more concentrated on pairs within C1 and C3. In particular, the three corpus callosum tracts, the body of the corpus callosum (BCC), GCC and SCC, showed consistently strong genetic correlations for each DTI parameter, except MO, which had few significant

genetic correlations, representing a pattern that was distinct from those of the other DTI parameters.

The role of sample size in SNP heritability estimation

We conducted the same SNP heritability analysis in the PNC and PING datasets, for which the sample sizes were much smaller than that of the UK Biobank. **Fig. 6** compares the SNP heritability of all common autosomal SNPs for the 21 main WM tracts obtained from the UK Biobank, PNC and PING datasets. The standard errors and adjusted p-values from the one-sided likelihood ratio tests are given in **Supplementary Tables 2 and 3** for PNC and PING, respectively. Perhaps due to the smaller sample size, SNP heritability estimated in these two datasets had much larger variance compared to those in the UK Biobank for all seven DTI parameters. In addition, SNP heritability in the PING and PNC datasets tended to be close to the boundaries of its support (i.e., 1 or 0). Different from the UK Biobank data, few main WM tracts in the PING or PNC data had consistent SNP heritability across the seven DTI parameters. When we partitioned the genetic variation by chromosome, the evidence of a highly polygenic (or onmigenic) genetic architecture of DTI parameters was much weaker compared to what we observed in the UK Biobank data (**Supplementary Fig. 26**).

To further explore this phenomenon, we performed simulations to study the role of sample size in SNP heritability estimation. We examined the behavior of the restricted maximum likelihood (REML) estimator in variance-component analysis of LMMs under different ratios of sample size to the number of SNPs (SS ratio). Details of the simulation setups are provided in the Online Methods. We found that as the SS ratio decreased, though the REML estimator remained unbiased, the variance of the estimator increased rapidly. In the simulation study, when the SS ratio became 0.01, the variance of the REML estimator was too large for us to gain a reliable estimate (**Supplementary Fig. 27**).

Voxel-based analysis on TBSS skeleton

We selected the GCC, ACR, SCR, SLF and PLIC tracts to conduct voxel-based analysis on the TBSS skeleton. Our tract-based analysis for the seven DTI parameters showed that all five tracts are heritable. We first compared the empirical density of the tract-mean and voxel-wise values of different DTI parameters on the GCC tract across subjects (**Supplementary Fig. 28**), and found that the tract-mean and voxel-wise values of MO have quite different density shapes. **Supplementary Figs. 29-36** display the voxel-wise SNP heritability estimates on the selected TBSS skeleton. For each DTI parameter, the voxel-wise SNP heritability estimates are smaller than their tract-based estimates. In particular, MO showed small SNP heritability estimates on GCC, ACR, SCR, and SLF, which may be due to its non-Gaussian distribution of voxel-wise data. However, for the other DTI parameters, some findings from the voxel-based analysis were indeed consistent with those from the tract-based analysis. Voxel-based analysis also indicated that the selected tracts are heritable for FA, AD (L1), RD, MD, L2 and L3 (**Supplementary Figs. 37-38**). And some pairs of heritability estimates of DTI parameters were similar, such as those for FA and RD on GCC and PLIC (**Supplementary Figs. 39-40**).

DISCUSSION

Heritability analysis usually serves as the initial step in imaging genetics, providing the rationale for genetic association studies, which can identify specific genes and pathways involved in the phenotype of interest. However, heritability analysis alone is not sufficient to fully inform the design of such follow-up studies. Understanding the genetic architecture, i.e., the shape of genetic contributions to phenotypic variance, can provide important, complementary information. A large number of family-based neuroimaging studies have documented that WM tracts are essentially heritable across the lifespan. However, the landscape of genetic contributions to DTI parameters of WM microstructures remains largely unknown. Here, our application of LMMs with variance-component analysis (30, 31) on unrelated samples in the UK Biobank dataset revealed the genetic architecture of WM tracts. Multiple insights were uncovered, including the highly polygenic (or omnigenic) shape of genetic contributions, the enrichment of SNP heritability in CNS-cell-active chromatin regions, the similarity of

heritability of DTI parameters on WM tracts, and the symmetric pattern across the left and right hemispheres. We also examined sex-specific heritability, genetic correlations on pairs of DTI parameters and WM tracts, and the voxel-wise heritability on the TBSS skeleton.

Though SNP heritability estimation is viewed as a lower bound of narrow-sense heritability, our analyses with all common autosomal SNPs provided heritability estimates close to the ones reported in family-based studies (Table 1 of (24)), and verified that most of the WM tracts are significantly heritable, regardless of which DTI parameter was used. These results may suggest that Genome-wide association studies (GWAS) of DTI phenotypes using common genetic variants may be more informative than studies focused on rare variants. It can be expected that future genetic analysis on heritable WM tracts will facilitate gene exploration, risk prediction and heterogeneity dissection on WM microstructures as well as the associated diseases/disorders. Complex and commissural fibers generally have larger heritability than associative or projection fibers, and left/right symmetry of heritability was observed across the whole brain. No systematic sex-specific modification on SNP heritability was detected. Our results partitioning the genetic variation in each chromosome shed light on a highly polygenic (or omnigenic) genetic architecture for WM tracts, which is in parallel with the infinitesimal model (42). There is strong linear correlation between the chromosomal length and the aggregate SNP heritability that is accounted for by the chromosome; and longer chromosomes clearly tend to have higher SNP heritability than the short ones. This finding indicates that for GWAS of white matter integrity, large sample size will be needed to identify variants with relatively small individual effect size.

On the main WM tracts, our findings provide strong evidence for the enrichment of genetic signals in active chromatin regions, especially for those active in the CNS cell type. The bivariate analysis of several pairs of DTI parameters shows that the genetic correlation of two DTI parameters (such as L2 and L3) is highly associated with their phenotypic correlation across WM tracts, after adjusting for the effects of fixed covariates. That is, a large proportion of the similarity of two DTI parameters can be consistently explained by their genetic similarity (R^2 >60% for all pairs), which may

reflect the non-specificity of the diffusion parameters and these DTI parameters consistently share very similar genetic bases across WM tracts. Perhaps for more biologically relevant tissue parameters, such as free water, axon diameters, and disambiguated anisotropies, genetic similarity would be less high. The genetic correlation analysis on pairs of WM tracts also confirms a genetic link among WM tracts, especially for the set of complex or commissural fibers, such as corpus callosum tracts BCC, GCC and SCC.

Our heritability analyses reflect several methodological limitations of the current approaches on population-based imaging genetic studies. First, similar to previous studies (23), CST and FX were reported to have low SNP heritability, which may be due to the fact that such small, tubular tracts cannot be well registered and reliably resolved with current techniques (43). Second, heritability estimated by SNP data reflects narrow-sense heritability, which only considers the additive genetic effects of common variants. The genetic architecture may change as we broadly consider all genetic contributions (such as rare variants and non-additive effects) in future studies. However, it is notable that with common autosomal SNPs (MAF> 0.01) in the UK Biobank, we have gained heritability estimates comparable to those reported in family-based studies. We performed simulations to verify that the REML estimator commonly used in LMM-based approaches requires a relatively large SS ratio. In practice, when we applied the SNP heritability approach to the PING and PNC datasets, we observed no significant findings. Similar concerns were mentioned in our previous report (44) on brain regional volumes. Although our simulations demonstrate the importance of sample size, it is also important to note that UK Biobank are primarily middle-aged/elderly samples while the PNC and PING cohorts are primarily adolescents. Very different processes are at play on the WM tracts for different datasets. For example, the myelin damage and loss, inflammation, as well as axonal shrinkage are ongoing on UK Biobank samples; on the other hand, myelination and axonal elimination occur in PNC and PING cohorts. Adjusting for age separately in each dataset may not be enough to fully account for the aging heterogeneity of these datasets. Therefore, the heritability differences among datasets should be interpreted with caution. In addition, though the omnigenic model has been theoretically developed and can help explain the genetic architecture of many complex human traits

(28, 45, 46), more rigorous validations are needed to confirm this hypothesis. Finally, our tract-based and voxel-based analyses on the MO parameter indicate that the LMM-based SNP heritability estimation may be sensitive to the distribution of the phenotypes. LMMs may have poor performance on non-Gaussian distributed phenotypes such as MO voxel values. With sample sizes increasing in population-based studies, future research will be required to overcome these limitations and improve our biological understanding of the human brain.

URLs.

ENIGMA-DTI: http://enigma.ini.usc.edu/protocols/dti-protocols/;

Plink2, https://www.cog-genomics.org/plink2/ ;

GCTA, http://cnsgenomics.com/software/gcta/ ;

BOLT-LMM, https://data.broadinstitute.org/alkesgroup/BOLT-LMM/ ;

MaCH-Admix, http://www.unc.edu/~yunmli/MaCH-Admix ;

LD Score Regression, https://github.com/bulik/ldsc/ ;

1000 Genomes, http://www.internationalgenome.org/ ;

UK Biobank, http://www.ukbiobank.ac.uk/resources/ ;

PING, http://pingstudy.ucsd.edu/resources/genomics-core.html ;

PNC,

https://www.ncbi.nlm.nih.gov/projects/gap/cgi-bin/study.cgi?study_id=phs000607.v1.p1;

Connectopedia Knowledge Database, http://www.fmritools.com/kdb/;

Mango, http://ric.uthscsa.edu/mango/;

BrainNet Viewer, https://www.nitrc.org/projects/bnv/.

METHODS

Methods are available in the ***Online Methods*** section.

Note: One supplementary information pdf file and one supplementary Excel file are available.

ACKNOWLEDGEMENTS

This research was partially supported by U.S. NIH grants MH086633 and MH092335, NSF grants SES-1357666 and DMS-1407655, a grant from the Cancer Prevention Research Institute of Texas, and the endowed Bao-Shan Jing Professorship in Diagnostic Imaging. We thank the individuals represented in the UK Biobank, PING and PNC datasets for their participation and the research teams for their work in collecting, processing and disseminating these datasets for analysis. This research has been conducted using the UK Biobank resource (application number 22783), subject to a data transfer agreement. Part of the data collection and sharing for this project was funded by the Pediatric Imaging, Neurocognition and Genetics Study (PING) (U.S. National Institutes of Health Grant RC2DA029475). PING is funded by the National Institute on Drug Abuse and the Eunice Kennedy Shriver National Institute of Child Health & Human Development. PING data are disseminated by the PING Coordinating Center at the Center for Human Development, University of California, San Diego. Support for the collection of the PNC datasets was provided by grant RC2MH089983 awarded to Raquel Gur and RC2MH089924 awarded to Hakon Hakonarson. All PNC subjects were recruited through the Center for Applied Genomics at The Children's Hospital in Philadelphia.

AUTHOR CONTRIBUTIONS

H.Z., B.Z., J.Z., R.S., Y.L., T.N., P.T., J.I. designed the study. B.Z. and J.Z. performed the experiments and analyzed the data. T.L., Y.S., Z.Z., F.Z., and H.L. downloaded the datasets, preprocessed MRI data, undertook the quantity controls and imputed SNP data. B.Z., H.Z., J.Z., R.S., Y.L., T.N., P.T., J.I. wrote the manuscript with feedback from all authors.

COMPETETING FINANCIAL INTERESTS

The authors declare no competing financial interests.

REFERENCES

1. Penke L, Maniega SM, Murray C, Gow AJ, Hernández MCV, Clayden JD, et al. A general factor of brain white matter integrity predicts information processing speed in healthy older people. Journal of Neuroscience. 2010;30(22):7569-74.

2. Penke L, Maniega SM, Bastin M, Hernández MV, Murray C, Royle N, et al. Brain-wide white matter tract integrity is associated with information processing speed and general intelligence. Molecular psychiatry. 2012;17(10):955.

3. Tamnes CK, Østby Y, Walhovd KB, Westlye LT, Due-Tønnessen P, Fjell AM. Intellectual abilities and white matter microstructure in development: a diffusion tensor imaging study. Human brain mapping. 2010;31(10):1609-25.

4. Ritchie SJ, Bastin ME, Tucker-Drob EM, Maniega SM, Engelhardt LE, Cox SR, et al. Coupled changes in brain white matter microstructure and fluid intelligence in later life. Journal of Neuroscience. 2015;35(22):8672-82.

5. Ritchie SJ, Booth T, Hernández MdCV, Corley J, Maniega SM, Gow AJ, et al. Beyond a bigger brain: Multivariable structural brain imaging and intelligence. Intelligence. 2015;51:47-56.

6. Nir TM, Jahanshad N, Villalon-Reina JE, Toga AW, Jack CR, Weiner MW, et al. Effectiveness of regional DTI measures in distinguishing Alzheimer's disease, MCI, and normal aging. NeuroImage: clinical. 2013;3:180-95.

7. Voineskos AN. Genetic underpinnings of white matter 'connectivity': heritability, risk, and heterogeneity in schizophrenia. Schizophrenia research. 2015;161(1):50-60.

8. Sudre G, Choudhuri S, Szekely E, Bonner T, Goduni E, Sharp W, et al. Estimating the Heritability of Structural and Functional Brain Connectivity in Families Affected by Attention-Deficit/Hyperactivity Disorder. JAMA psychiatry. 2017;74(1):76-84.

9. Vogel K, Timmers I, Kumar V, Nickl-Jockschat T, Bastiani M, Roebroek A, et al. White matter microstructural changes in adolescent anorexia nervosa including an exploratory longitudinal study. NeuroImage: Clinical. 2016;11:614-21.

10. Basser PJ, Mattiello J, LeBihan D. Estimation of the effective self-diffusion tensor from the NMR spin echo. Journal of Magnetic Resonance, Series B. 1994;103(3):247-54.

11. Beaulieu C. The basis of anisotropic water diffusion in the nervous system–a technical review. NMR in Biomedicine. 2002;15(7-8):435-55.

12. Thomason ME, Thompson PM. Diffusion imaging, white matter, and psychopathology. Annual review of clinical psychology. 2011;7.

13. Jones DK, Knösche TR, Turner R. White matter integrity, fiber count, and other fallacies: the do's and don'ts of diffusion MRI. Neuroimage. 2013;73:239-54.

14. Cox SR, Ritchie SJ, Tucker-Drob EM, Liewald DC, Hagenaars SP, Davies G, et al. Ageing and brain white matter structure in 3,513 UK Biobank participants. Nature communications. 2016;7:13629.

15. Smith SM, Jenkinson M, Johansen-Berg H, Rueckert D, Nichols TE, Mackay CE, et al. Tract-based spatial statistics: voxelwise analysis of multi-subject diffusion data. Neuroimage. 2006;31(4):1487-505.

16. Tamnes CK, Roalf DR, Goddings A-L, Lebel C. Diffusion MRI of white matter microstructure development in childhood and adolescence: methods, challenges and progress. Developmental cognitive neuroscience. 2017.

17. Geng X, Gouttard S, Sharma A, Gu H, Styner M, Lin W, et al. Quantitative tract-based white matter development from birth to age 2years. Neuroimage. 2012;61(3):542-57.

18. Lee SJ, Steiner RJ, Luo S, Neale MC, Styner M, Zhu H, et al. Quantitative tract-based white matter heritability in twin neonates. NeuroImage. 2015;111:123-35.

19. Lee SJ, Steiner RJ, Yu Y, Short SJ, Neale MC, Styner MA, et al. Common and heritable components of white matter microstructure predict cognitive function at 1 and 2 y. Proceedings of the National Academy of Sciences. 2017;114(1):148-53.

20. Brouwer RM, Mandl RC, Peper JS, van Baal GCM, Kahn RS, Boomsma DI, et al. Heritability of DTI and MTR in nine-year-old children. Neuroimage. 2010;53(3):1085-92.

21. Brouwer RM, Mandl RC, Schnack HG, van Soelen IL, van Baal GC, Peper JS, et al. White matter development in early puberty: a longitudinal volumetric and diffusion tensor imaging twin study. PloS one. 2012;7(4):e32316.

22. Chiang M-C, Barysheva M, Toga AW, Medland SE, Hansell NK, James MR, et al. BDNF gene effects on brain circuitry replicated in 455 twins. Neuroimage. 2011;55(2):448-54.

23. Kochunov P, Jahanshad N, Marcus D, Winkler A, Sprooten E, Nichols TE, et al. Heritability of fractional anisotropy in human white matter: a comparison of Human Connectome Project and ENIGMA-DTI data. Neuroimage. 2015;111:300-11.

24. Vuoksimaa E, Panizzon MS, Hagler Jr DJ, Hatton SN, Fennema-Notestine C, Rinker D, et al. Heritability of white matter microstructure in late middle age: A twin study of

tract-based fractional anisotropy and absolute diffusivity indices. Human brain mapping. 2017;38(4):2026-36.

25. Kanchibhotla SC, Mather KA, Wen W, Schofield PR, Kwok JB, Sachdev PS. Genetics of ageing-related changes in brain white matter integrity–A review. Ageing research reviews. 2013;12(1):391-401.

26. Timpson NJ, Greenwood CM, Soranzo N, Lawson DJ, Richards JB. Genetic architecture: the shape of the genetic contribution to human traits and disease. Nature Reviews Genetics. 2017.

27. Badano JL, Katsanis N. Beyond Mendel: an evolving view of human genetic disease transmission. Nature reviews Genetics. 2002;3(10):779.

28. Boyle EA, Li YI, Pritchard JK. An Expanded View of Complex Traits: From Polygenic to Omnigenic. Cell. 2017;169(7):1177-86.

29. Sudlow C, Gallacher J, Allen N, Beral V, Burton P, Danesh J, et al. UK biobank: an open access resource for identifying the causes of a wide range of complex diseases of middle and old age. PLoS medicine. 2015;12(3):e1001779.

30. Yang J, Lee SH, Goddard ME, Visscher PM. GCTA: a tool for genome-wide complex trait analysis. The American Journal of Human Genetics. 2011;88(1):76-82.

31. Loh P-R, Bhatia G, Gusev A, Finucane HK, Bulik-Sullivan BK, Pollack SJ, et al. Contrasting genetic architectures of schizophrenia and other complex diseases using fast variance-components analysis. Nature genetics. 2015;47(12):1385-92.

32. Bulik-Sullivan BK, Loh P-R, Finucane HK, Ripke S, Yang J, Patterson N, et al. LD Score regression distinguishes confounding from polygenicity in genome-wide association studies. Nature genetics. 2015;47(3):291-5.

33. Visscher PM, Hill WG, Wray NR. Heritability in the genomics era—concepts and misconceptions. Nature Reviews Genetics. 2008;9(4):255-66.

34. Yang J, Zeng J, Goddard ME, Wray NR, Visscher PM. Concepts, estimation and interpretation of SNP-based heritability. Nature genetics. 2017;49(9):1304.

35. Alfaro-Almagro F, Jenkinson M, Bangerter NK, Andersson JL, Griffanti L, Douaud G, et al. Image Processing and Quality Control for the first 10,000 Brain Imaging Datasets from UK Biobank. bioRxiv. 2017:130385.

36. Thompson PM, Stein JL, Medland SE, Hibar DP, Vasquez AA, Renteria ME, et al. The ENIGMA Consortium: large-scale collaborative analyses of neuroimaging and genetic data. Brain imaging and behavior. 2014;8(2):153-82.

37. Finucane HK, Bulik-Sullivan B, Gusev A, Trynka G, Reshef Y, Loh P-R, et al. Partitioning heritability by functional annotation using genome-wide association summary statistics. Nature genetics. 2015;47(11):1228-35.

38. Satterthwaite TD, Elliott MA, Ruparel K, Loughead J, Prabhakaran K, Calkins ME, et al. Neuroimaging of the Philadelphia neurodevelopmental cohort. Neuroimage. 2014;86:544-53.

39. Jernigan TL, Brown TT, Hagler DJ, Akshoomoff N, Bartsch H, Newman E, et al. The pediatric imaging, neurocognition, and genetics (PING) data repository. Neuroimage. 2016;124:1149-54.

40. Benjamini Y, Hochberg Y. Controlling the false discovery rate: a practical and powerful approach to multiple testing. Journal of the royal statistical society Series B (Methodological). 1995:289-300.

41. Hu Y, Lu Q, Powles R, Yao X, Yang C, Fang F, et al. Leveraging functional annotations in genetic risk prediction for human complex diseases. PLOS Computational Biology. 2017;13(6):e1005589.

42. Fisher RA. XV.—The correlation between relatives on the supposition of Mendelian inheritance. Earth and Environmental Science Transactions of the Royal Society of Edinburgh. 1919;52(2):399-433.

43. Bach M, Laun FB, Leemans A, Tax CM, Biessels GJ, Stieltjes B, et al. Methodological considerations on tract-based spatial statistics (TBSS). Neuroimage. 2014;100:358-69.

44. Zhao B, Ibrahim JG, Li Y, Li T, Wang Y, Shan Y, et al. Heritability of regional brain volumes in large-scale neuroimaging and genetic studies. bioRxiv. 2017:208496.

45. Chen C-H, Peng Q, Schork AJ, Lo M-T, Fan C-C, Wang Y, et al. Large-scale genomics unveil polygenic architecture of human cortical surface area. Nature communications. 2015;6:7549.

46. Shi H, Kichaev G, Pasaniuc B. Contrasting the genetic architecture of 30 complex traits from summary association data. The American Journal of Human Genetics. 2016;99(1):139-53.

47. Miller KL, Alfaro-Almagro F, Bangerter NK, Thomas DL, Yacoub E, Xu J, et al. Multimodal population brain imaging in the UK Biobank prospective epidemiological study. Nature neuroscience. 2016;19(11):1523-36.

48. Jenkinson M, Beckmann CF, Behrens TE, Woolrich MW, Smith SM. Fsl. Neuroimage. 2012;62(2):782-90.

49. Andersson JL, Sotiropoulos SN. An integrated approach to correction for off-resonance effects and subject movement in diffusion MR imaging. Neuroimage. 2016;125:1063-78.

50. Smith SM. Fast robust automated brain extraction. Human brain mapping. 2002;17(3):143-55.

51. Davis LK, Yu D, Keenan CL, Gamazon ER, Konkashbaev AI, Derks EM, et al. Partitioning the heritability of Tourette syndrome and obsessive compulsive disorder reveals differences in genetic architecture. PLoS genetics. 2013;9(10):e1003864.

52. Purcell S, Neale B, Todd-Brown K, Thomas L, Ferreira MA, Bender D, et al. PLINK: a tool set for whole-genome association and population-based linkage analyses. The American Journal of Human Genetics. 2007;81(3):559-75.

53. Liu EY, Li M, Wang W, Li Y. MaCH-Admix: genotype imputation for admixed populations. Genetic epidemiology. 2013;37(1):25-37.

54. Consortium GP. An integrated map of genetic variation from 1,092 human genomes. Nature. 2012;491(7422):56-65.

55. Lee SH, DeCandia TR, Ripke S, Yang J, Sullivan PF, Goddard ME, et al. Estimating the proportion of variation in susceptibility to schizophrenia captured by common SNPs. Nature genetics. 2012;44(3):247-50.

56. Gu Z, Gu L, Eils R, Schlesner M, Brors B. circlize implements and enhances circular visualization in R. Bioinformatics. 2014;30(19):2811-2.

ONLINE METHODS

Participants and image preprocessing

Datasets used in this paper are the UK Biobank, PNC, and PING. Detailed data collection/processing procedures and quality control prior to the release of data are documented at http://www.ukbiobank.ac.uk/resources/ for the UK Biobank, http://pingstudy.ucsd.edu/resources/genomics-core.html for PING and https://www.ncbi.nlm.nih.gov/projects/gap/cgi-bin/study.cgi?study_id=phs000607.v1.p1 for PNC. For each dataset, we used subjects with both DTI and SNP data available after applying proper quality controls (see below).

DTI datasets of the UK Biobank were acquired at the 2*2*2 mm spatial resolution with multiband acceleration factor of three (i.e., three slices are acquired simultaneously) and two b-values (b = 1,000 and 2,000 s/mm^2), anterior-to-posterior (AP) is the acquisition phase-encoding direction. For each of these b-values, 50 diffusion-encoding directions were acquired, and there were 100 distinct directions in total. The echo time (TE) was 92 ms and the repetition time (TR) was 3600 ms. The diffusion preparation was a standard (mono-polar) Stejskal-Tanner pulse sequence. The shorter echo time (TE = 92 ms) can enable a higher signal-to-noise ratio (SNR) than a twice-refocused (bipolar) sequence at the expense of stronger eddy current distortions (47). We ran the TBSS-ENIGMA pipeline (36) on DTIs with the FSL tool set (48). For DTI with a given diffusion strength (b-values) and direction of the magnetic diffusion gradient (q-vectors), we first conducted eddy correction (49), extracted the brain (50), and then fit a diffusion tensor model (10) to obtain a scalar DTI map of FA, L1 (AD), L2, L3, MD, MO, and RD. We excluded subjects whose FA images did not pass the standard imaging quality controls, and removed outliers. Second, we used linear registration to register each of the FA images to the Enigma FA template at 1*1*1 mm spatial resolution. We performed quality controls again after registration and excluded subjects with bad registration. Next, we applied nonlinear registration to align the linearly registered FA images to the ENIGMA FA template and masked the registered FA with a template mask. Finally, we projected the ENIGMA skeleton onto the registered FA images to skeletonize them and extract ROI-based FA statistics. By transferring the individual L1, L2, L3, MD, MO, and RD images to the FA template space, we obtained both voxel-wise skeleton and ROI-based statistics of all these DTI parameters. An overview of our DTI pipeline is given in **Supplementary Fig. 41**. The demographic information for the DTI datasets is listed in

Supplementary Table 4. The DTI dataset description for PNC and PING are described in (38) and (39), respectively.

Genotyping

Genotype imputation was performed on the PNC and PING datasets. For the UK Biobank, we used an unimputed SNP dataset, because the imputed SNP dataset has not been released when we performed this study. We may obtain higher heritability estimates in UK Biobank if imputed SNP data were available. However, previous study has found that imputed SNP data did not show significant increases in SNP heritability estimation (51). Standard quality controls were performed to ensure high quality of the SNP data. These procedures were performed using the Plink tool set (52).

PNC Imputation

From the PNC database, 8722 participants were genotyped on one of the six different platforms: 66 were genotyped on the Affymetrix array 6.0; 722 were genotyped on the Axiom array; 556 were genotyped on the Illumina HumanHap 550 array version 1; 1914 were genotyped on the Illumina HumanHap 550 array version 3; 1657 were genotyped on the Illumina HumanHap 610 array; and 3807 were genotyped on the Illumina Human Omni Express array. We applied the quality control steps to each dataset separately, which included removal of subjects with more than 10% missing values, removal of SNPs (i) with more than 5% missing values, (ii) with MAF smaller than 5%, (iii) with Hardy-Weinberg equilibrium test p-value $< 1*10^{-6}$, and (iv) located on a sex chromosome. We then employed MACH-Admix software (53) to perform genotype imputation, using 1000G Phase I Integrated Release Version 3 haplotypes (54) as a reference panel. We also conducted quality control after imputation, excluding markers with (i) low imputation accuracy (based on imputation output R^2); and (ii) Hardy-Weinberg equilibrium test p-value $< 1*10^{-6}$. We combined the six datasets and retained the shared SNPs. Finally, 5,354,265 bi-allelic markers (including SNPs and indels) from 8681 subjects remained for further analysis.

PING Imputation

We applied the following preprocessing technique to the genetic data. The first-line quality control steps were (i) call rate check per subject and per SNP marker, (ii) sex check, and (iii) sibling pair identification. The second-line preprocessing steps were removal of SNPs (i) with more than 5% missing values, (ii) with MAF smaller than 10%, (iii) with Hardy-Weinberg equilibrium p-value < $1*10^{-6}$, and (iv) located on a sex chromosome. We thus had 539,865 SNPs from 1036 subjects for further processing. We employed MACH-Admix software (53) to perform genotype imputation, using 1000G Phase I Integrated Release Version 3 haplotypes (54) as a reference panel. We also conducted quality control after imputation, excluding markers with (i) low imputation accuracy (based on imputation output R^2), and (ii) Hardy-Weinberg equilibrium p-value < $1*10^{-6}$. Finally, 10,883,584 bi-allelic markers (including SNPs and indels) from 1036 subjects were retained for data analysis.

Quality control on UK Biobank, PING and PNC

On each SNP dataset, we further selected subjects with available DTI data. We then used all autosomal SNPs and again applied the standard quality control procedures: excluding subjects with more than 10% missing genotypes, only including SNPs with MAF > 0.01, with genotyping rate > 90%, and passing Hardy-Weinberg test (P > $1*10^{-7}$). We further removed non-European subjects, if any. In PING, we only used biologically unrelated subjects. After quality control, we calculated the GRM by all SNPs and by SNPs on each chromosome separately using the GCTA tool set (30). To avoid including closely related relatives, we excluded one of any pair of individuals with estimated genetic relationship larger than 0.025. The sample sizes of the datasets after conducting all quality control procedures are listed in **Supplementary Table 5**.

Heritability analysis

First, for each DTI parameter, we estimated the proportion of variation explained by all autosomal SNPs with a LMM in each WM tract. There are 63 tracts (21 main tracts and 42 sub-tracts) and seven DTI parameters. The formal setting of the LMM and definition of likelihood ratio test statistics can be found in (30). The basic idea is to fit the GRM with random effects to the phenotypic measure, while adjusting for other covariates with

fixed effects. The GRM was the correlation matrix of participants estimated by the common genetic variants, which was expected to capture the genetic similarity among unrelated individuals. Then the heritability of a phenotype was estimated by contrasting the genetic similarity among individuals with their phenotypic similarity. Baseline age, gender indicator, and the top 10 principal components of GRM were included as covariates. Besides the combined sample, we fitted the LMM separately on female and male samples in the UK Biobank dataset. Voxel-wise skeleton analysis was performed on selected heritable main WM tracts. Second, we partitioned the genetic variation by each chromosome. We estimated the GRM of each chromosome and fitted each of them separately on each tract and each DTI parameter. The same set of covariates was included in these LMMs. Next, in each tract, we performed bivariate genetic correlation analysis for the set of DTI parameters L1 (AD), L2, L3 and the set FA, RD, MD, MO. The formal setting of the bivariate LMM and definition of genetic correlation can be found in (31, 55). Similarly, we performed pairwise genetic correlation analysis on the main WM tracts for each of the DTI parameters.

Finally, we fitted linear models between the length of a chromosome and the aggregate heritability across all WM tracts and all DTI parameters. We further ordered and clustered the 22 chromosomes into three groups according to their lengths: long (CHRs 2, 1, 6, 3), medium (CHRs 4,5,7,8,10,11), and short (the other CHRs). We also clustered the tracts according to their biological functions. The heritability distribution across these communities was displayed using the R package circlize (56).

Functional annotation of genetic signals

We obtained cell-type-specific active chromatin annotations per SNP from (37) and (28). According to (37), we performed functional annotation analyses using cell-type-specific annotations marked by four histones: H3K4me1, H3K4me3, H3K9ac and H3K27ac. Each cell-type-specific annotation corresponded to a histone mark in a single cell type, and there were 220 such annotations. The 220 cell-type-specific annotations were further divided into ten groups, including adrenal gland and pancreas, CNS, cardiovascular system, connective tissue and bone, gastrointestinal, immune and hematopoietic systems,

kidney, liver, skeletal muscle and other. The SNPs were divided into three non-overlapping groups according to their activeness in the ten cell-type groups: CNS_active, CNS_inactive and always_inactive. A SNP was labeled "CNS_active" if it was annotated as active in the CNS cell-type group. A SNP was labeled "CNS_inactive" if it was annotated as inactive in the CNS cell-type group, but was active in at least one of the other cell-type groups, and SNPs that were not active in any cell type were labeled "always_inactive". As the number of SNPs in each group was different, we randomly selected the same number of SNPs from each cell group and computed the heritability for each group in each tract. We generated 50 randomly selected SNP datasets and calculated the mean of these 50 heritability estimates in each tract.

Data availability

Links to all datasets (UK Biobank, PNC and PING) that support the findings of this study are provided in the URL section. Researchers can apply to use these datasets for health-related research that is in the public interest.

Figure Legends

Figure 1. SNP heritability of 21 main WM tracts grouped by tract functions from the UK Biobank dataset.

Figure 2. SNP heritability of 21 main WM tracts from the UK Biobank dataset.

Figure 3. SNP heritability of 21 main WM tracts by each chromosome from the UK Biobank dataset.

Figure 4. SNP heritability of 21 main WM tracts by category of SNPs according to CNS functional annotations from the UK Biobank dataset.

Figure 5. Genetic correlation in pairs of main WM tracts grouped by tract functions.

Figure 6. Comparing SNP heritability of 21 main WM tracts from the UK Biobank, PING and PNC datasets.

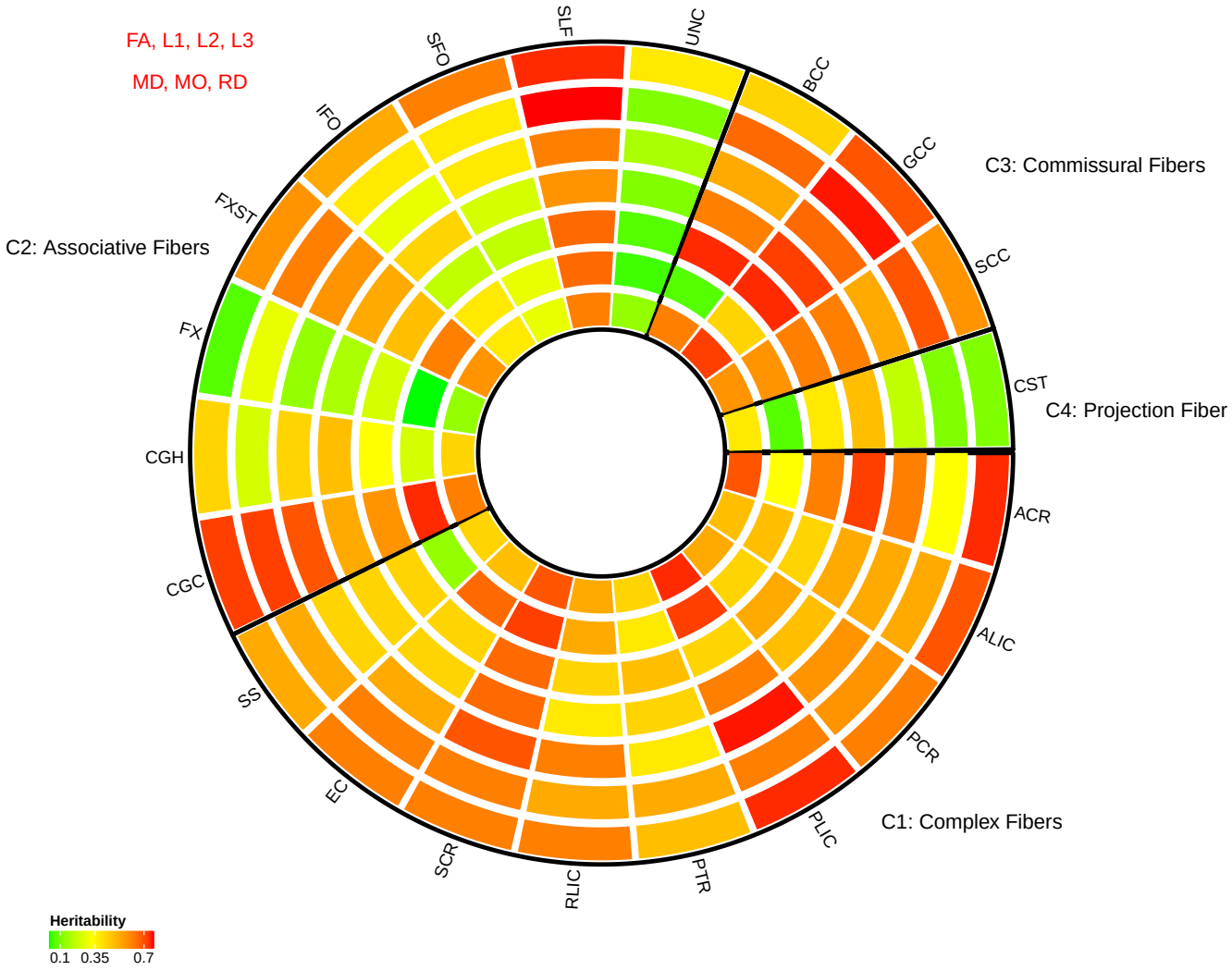

Figure 1: SNP heritability of 21 main WM tracts grouped by tract functions from the UK Biobank dataset.

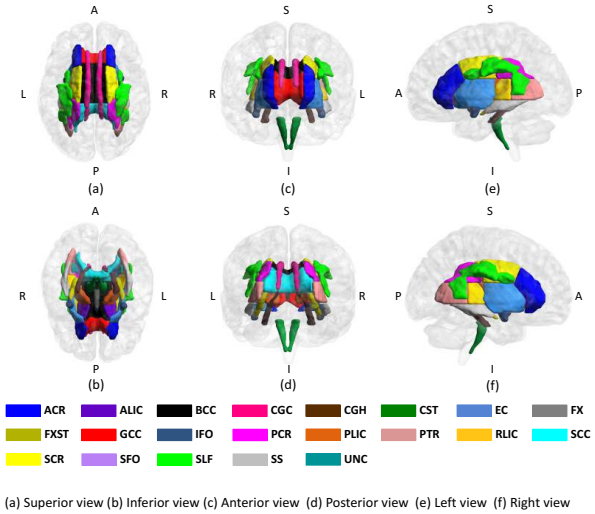

(a) WM Main Tracts Annotation

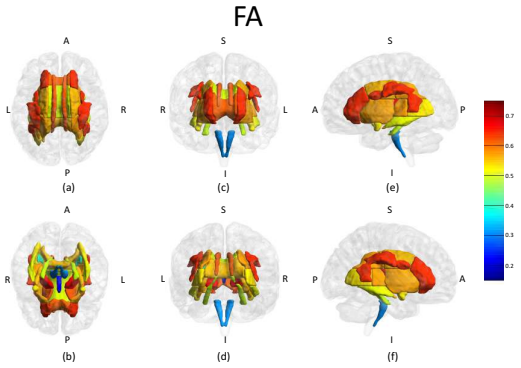

(b)

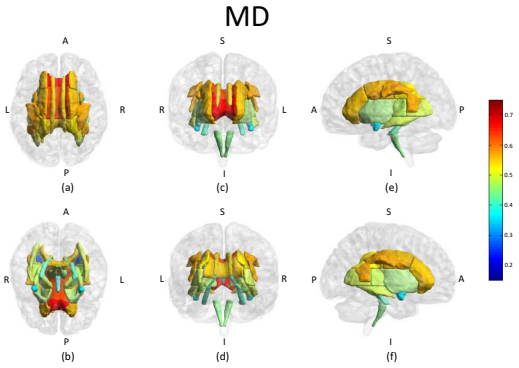

(c)

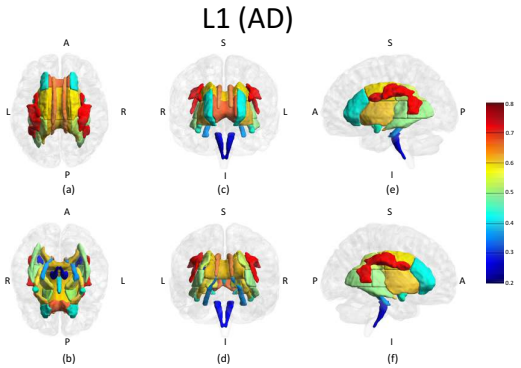

(d)

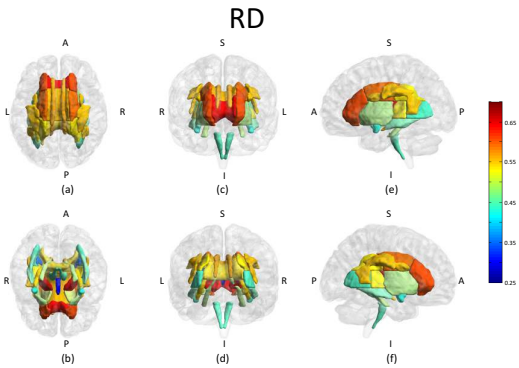

(e)

Figure 2: SNP heritability of 21 main WM tracts from the UK Biobank dataset.

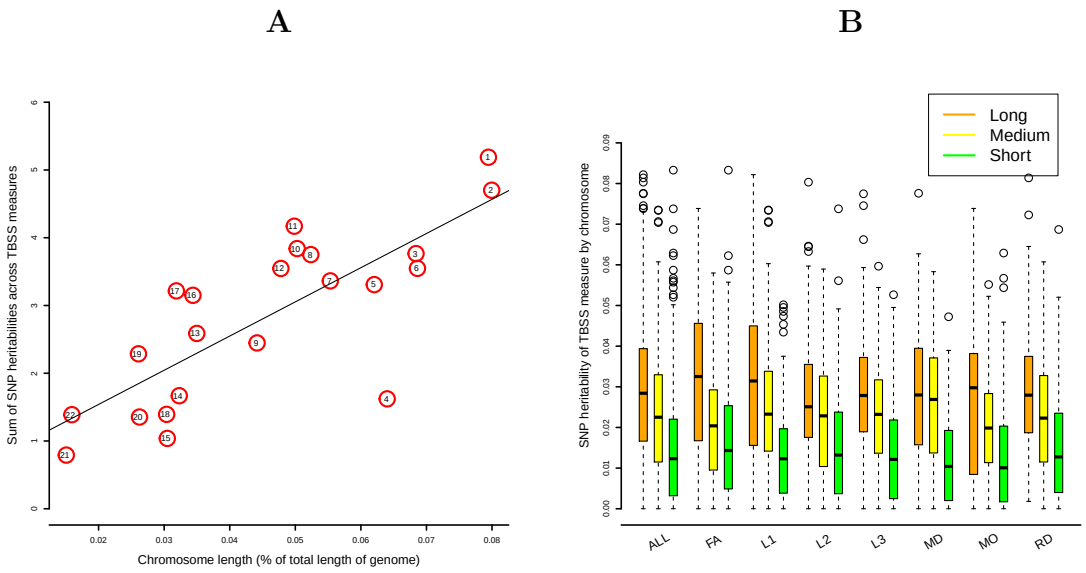

(a) Aggregated SNP heritability of each chromosome.

(b) SNP heritability grouped by chromosome length.

Figure 3: SNP heritability of 21 main WM tracts by each chromosome from the UK Biobank dataset.

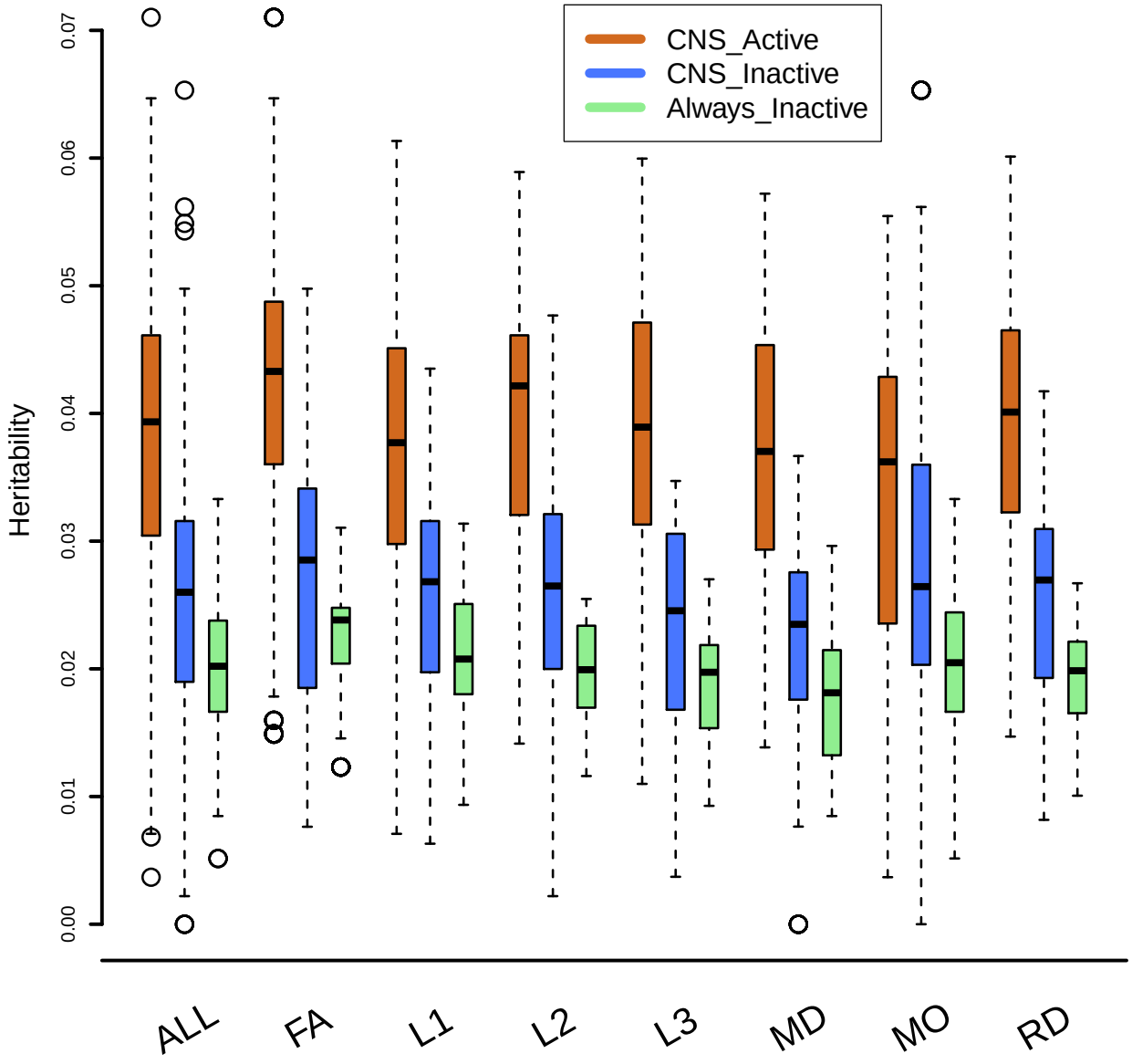

Figure 4: SNP heritability of 21 main WM tracts by category of SNPs according to CNS functional annotations from the UK Biobank dataset.

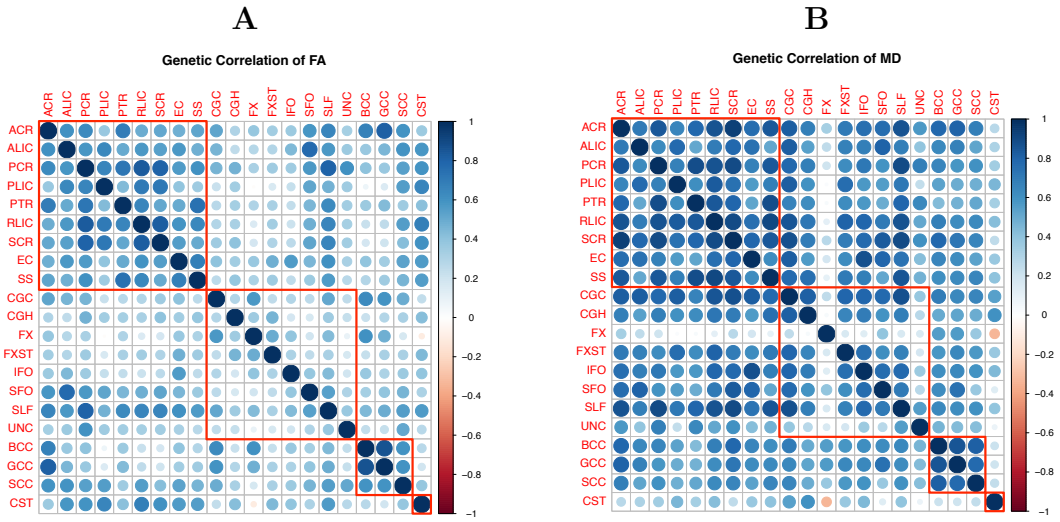

(a) FA **(b)** MD

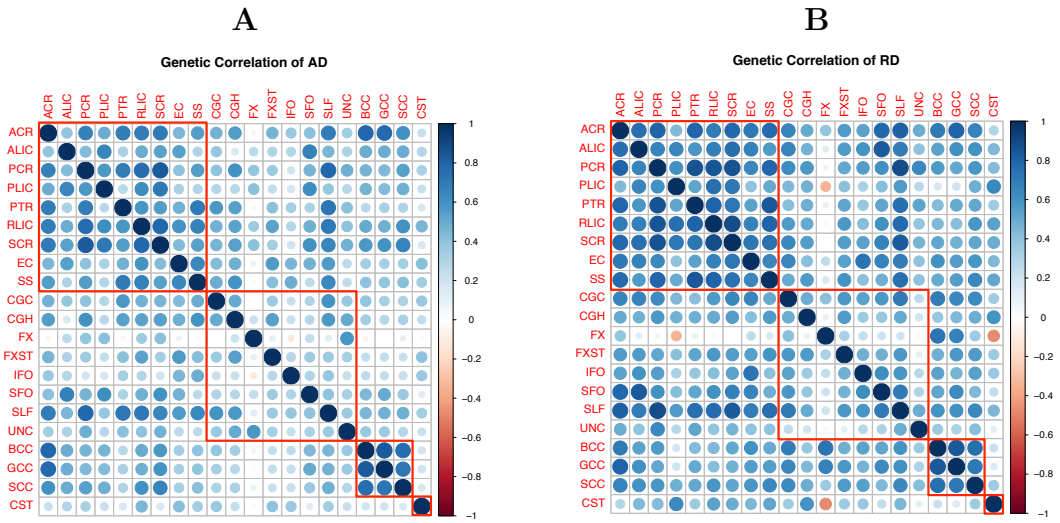

(c) L1 (AD) **(d)** RD

Figure 5: Genetic correlation in pairs of main WM tracts grouped by tract functions.

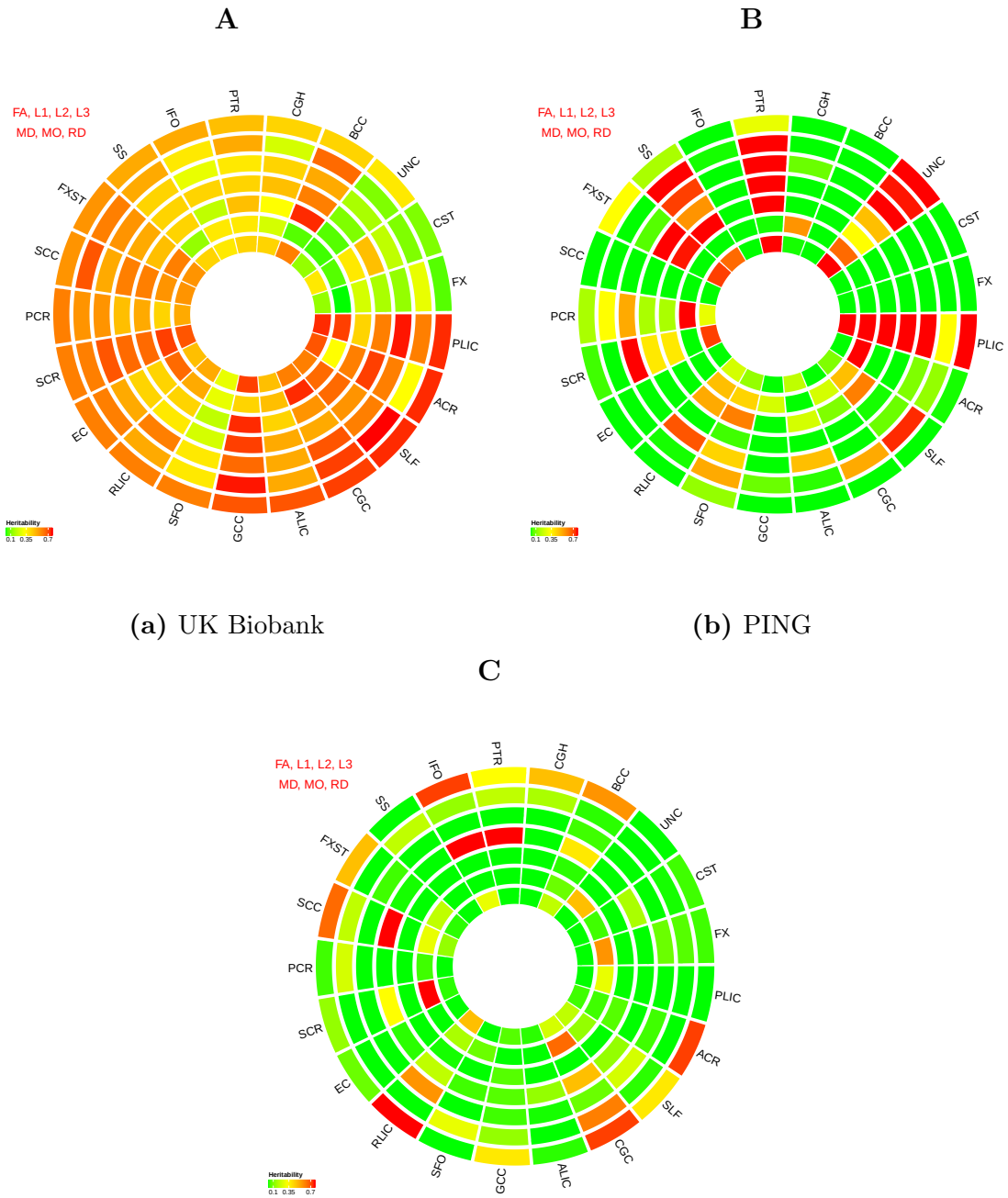

(a) UK Biobank

(b) PING

(c) PNC

Figure 6: Comparing SNP heritability of 21 main WM tracts from the UK Biobank, PING and PNC datasets.